Importance of whispering gallery resonances for nuclear scattering from weakly bound or unstable nuclei

Alan C. Shotter*
School of Physics and Astronomy, University of Edinburgh, JCMB, Peter Guthrie Tait Road, Edinburgh EH9 3FD, United Kingdom

Alessia Di Pietro†
INFN, Laboratori Nazionali del Sud, via S. Sofia 62, 1-95123 Catania, Italy

(Received 20 June 2024; accepted 13 August 2024; published 5 September 2024)

Internal surface standing wave resonances can occur when either electromagnetic or acoustic waves interact with cylindrical or spherical material structures. These resonances are often termed whispering gallery resonances, a reference to the focusing of sound within a cylindrical gallery. Here, a report is presented of an investigation to establish the importance of such surface standing wave resonances for nuclear wave scattering from unstable or weakly bound nuclei. To facilitate the investigation an analytical model, the transitional rotational model, has been developed to probe the occurrence of whispering gallery phenomena within nuclear wave scattering. Understanding such phenomena can be relevant when nuclear structure information are derived from scattering experiments. Moreover, it can also be important for the understanding of nuclear pathways leading to stellar explosions.

DOI: 10.1103/PhysRevC.110.034603

I. INTRODUCTION

The propagation of wave energy can be strongly influenced by any reflecting and absorbing structures the wave encounters. Obviously, this is an important consideration, for example, in the design of auditoria, where sound wave energy distribution is of prime importance. An interesting example of sound energy propagation, linked to reflecting structures, is the so-called whispering gallery phenomenon. When a whisper is directed near to a circular wall, then someone on the opposite side of the structure can clearly hear the whisper, even though the two people may be separated by a large distance. This phenomenon was first analyzed mathematically by Rayleigh in 1878 [1]. Essentially, the sound wave energy, by reflection, is confined to the circular surface of the gallery wall, undergoing only a small reduction of the original intensity. How sound waves interact with different configurations of materials has been of continued interest, especially the interaction with a spherical shell of material [2,3].

An analogy of the whispering gallery phenomenon has also been observed in optical systems, and is now developing into a whole new area of research. When light encounters transparent cylindrical or spherical structures, part of the light can be trapped and concentrated within and outside the structure [4]. This type of light scattering from spheres or cylinders is termed Mie scattering, named after the person who first used Maxwell's electromagnetic equations to solve the scattering problem [5]. An illustration of such light scattering from a transparent sphere, comprising a core and shell of different refractive indexes, is shown in Fig. 1. This shows standing-wave structures within the shell produced by wave interference in the shell. Since this trapping of wave energy is dependent on how it interacts with symmetrical geometrical structures, it must be quite general. Therefore, the question arises, could this trapping phenomenon occur for other types of waves other than acoustic or electromagnetic? Interestingly, quantum whispering gallery effects can occur in the case of matter waves, as in cold neutron scattering by a perfect cylindrical mirror, with the neutron particle waves affected by a large centrifugal acceleration [8].

In nuclear physics, the scattering of particle waves of two interacting nuclei in general involves multinucleon interactions between the constituent nuclei. However, for a simple reaction process, such as elastic scattering, it is possible to derive the particle scattering wave function by solving the Schrödinger equation with a simple effective potential related to the nuclear mean density profile of the two reacting nuclei. The mean nuclear density profile for stable nuclei is almost uniform within the nucleus surface, but rapidly falls off beyond. However, for some weakly bound nuclei such as ^{9}Be, or unstable nuclei such as ^{9}Li, density fall off is less rapid. Indeed, in some cases this outer core region forms a distinct surface region called a halo [9–12]. Examples of halo nuclei are ^{6}He, ^{11}Be, or ^{11}Li. There is a general interest to study nuclear reactions involving very unstable nuclei, since they play a critical role in supernova and nova explosions. As a result, the debris ejected from such stellar events provide one of the critical paths for element evolution in the universe. So, investigating such nuclear reactions, either experimentally or theoretically, has great relevance beyond the field of nuclear physics [13].

*Contact author: Alan.Shotter@ed.ac.uk
†Contact author: dipietro@lns.infn.it

The consideration of how reacting nuclei are influenced by their surface regions has been a topic of interest for many years [14–23]. For example, early investigations of elastic scattering for reacting systems such as $^{12}C + ^{12}C$, and $^{16}O + ^{16}O$ found large fluctuations in cross section as a function of incident energy. These resonantlike structures have been interpreted as transient dinuclear systems formed by the two reacting nuclei linked by their surface interactions [24], and there has been a suggestion that these could be related to whispering-gallery-like phenomena [25]. Other theoretical and experimental investigations have also interpreted various specific elastic scattering reaction data as phenomena associated with surface interactions [14–23]. Scattering reactions involving unstable or weakly bound nuclei (which have distinct interaction regions between their cores and outer shells) interacting with a well bound nucleus, is analogous to light scattering from optical spheres, with shells of different refractive indexes. This paper attempts to answer the question as to whether trapping, i.e., partial orbiting, can occur within the shell region for this nuclear situation that results in whispering-gallery-like phenomena and its consequences on the reaction process and cross section. To help answer the question as to whether an increase of diffuseness results in more pronounced outer shell resonance phenomena, a simple elastic scattering model has been developed that specifically emphasizes the importance of an extended shell beyond the core. This model is then used to investigate how the scattering of an α particle, which is a well-bound nucleus with a sharp surface, will interact with nuclei, which have an outer low-density shell and, in turn, if data show evidence of whispering-gallery-like phenomena. In the next section, Sec. II, the theoretical outline of the model is presented. In Sec. III the TRM is applied to the $^{9}Li + ^{4}He$ scattering, together with a visualization of the reaction dynamics for an α-nucleus encounter. Section IV presents the results of using this model to investigate two other reactions involving α scattering from unstable ^{6}He and weakly bound ^{9}Be nuclei. A discussion is presented in Sec. V of the potential parameters extracted from the TRM analysis of the experimental data. Section VI reports the conclusions. In the Appendix the mathematical details of the model are reported.

II. DYNAMICS OF INTERACTING NUCLEI

The most important consideration in any reaction model is the nature of the potential interaction between the reacting participants. For low-energy elastic reactions, where there are only two strongly bound participants, the interaction potential is often assumed to be a square well rounded off at the nuclear surface [26,27]. Another approach, which is less phenomenological, is to assume that the interaction potential is related to the product of the nuclear densities of the approaching nuclei. These so-called folding potentials assume the nuclear density profiles of the two participant nuclei remain rigid during their interaction [28]. However, for nuclei that have a central core surrounded by an outer shell of weakly bound nucleons, the nuclear density distribution cannot be considered as rigid when interacting with other nuclei, i.e., the nuclear density shape will change. This so-called shape polarization has been known for some time. For example, Vasilevsky *et al.* [29], have studied the influence of this shape polarization on the outcomes of reactions involving weakly bound light nuclei. One reaction studied was $^{6}Li + p$ inelastic scattering. From this study, it is clear that the nuclear density distribution for ^{6}Li evolves continuously as the proton approaches. This will mean that the shape of the interaction potential also will continuously evolve. In the absence of knowledge of how this evolution occurs, in most studies it is assumed that the shape **does not** change, e.g., when using a phenomenological Woods-Saxon (W-S) potential. Essentially, it is being assumed that this represents an average shape for the potential over the interaction time. Nevertheless, the W-S potential has been used quite successfully for reactions involving well-bound stable nuclei, where the surfaces are well defined. However, it has been found that for scattering involving weakly bound nuclei, as for instance the unstable neutron-halo ^{11}Be nucleus, an extended shell potential had to be added to the volume W-S potential to be able to describe the unusual shape of the scattering angular distribution [30].

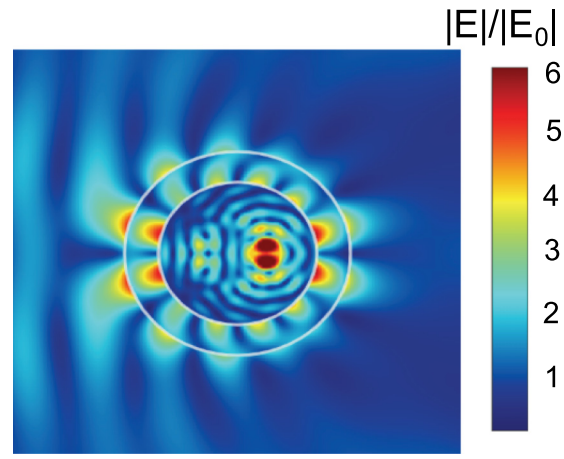

FIG. 1. Mie scattering from a core plus shell transparent sphere, showing the relative amplitude of the electric field. Light is incident from left to right. The core and shell have different refractive indexes. Diagram generated from online software [6,7].

So, in the present model, for a well-bound α particle scattering from an unstable or weakly bound nucleus, instead of a single W-S potential, a double W-S potential may be more appropriate, one associated with the core, the other with the outer shell. Since the second potential takes account of the outer shell, in order to further simplify the interaction, the surface diffusion coefficients of the two potentials are taken as zero; i.e., the two potentials have a squared form (see Fig. 2) Solving scattering problems with such square potentials has the advantage that the scattering wave functions and cross sections can be derived in analytical form. Since the model aims to highlight the importance of transient orbiting, resulting from outer shell nucleon interactions, it is termed the transitional rotational model (TRM) the analytical formalism for which is given in the Appendix. This is a simple model, but it is interesting to see how far it can represent experimental data.

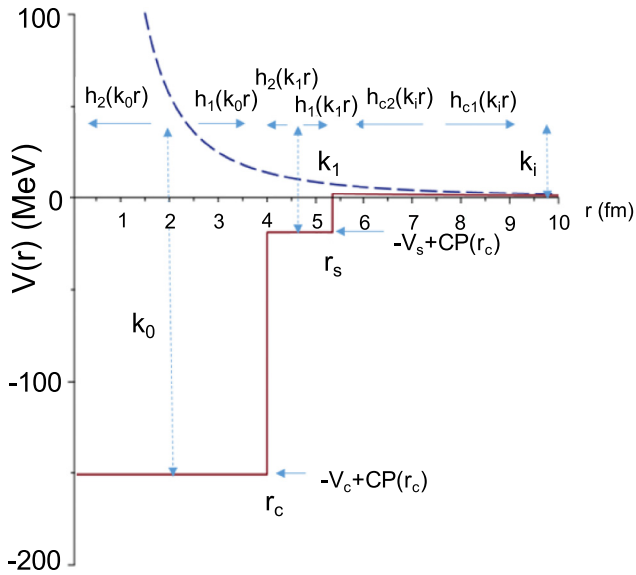

FIG. 2. Shows the nuclear core potential, $V_c = V_r + iV_i$, where V_r is the real part and V_i is the imaginary part of the potential. V_s is the shell potential, and CP the Coulomb potential. The form of the $h_{1,(2)}$ functions will strongly depend on the orbital angular momentum quantum number l. The k symbols represent the wave numbers in the different regions. The values of the potentials represented here are deduced from the TRM that best matches the experimental cross sections for the elastic ^{9}Be(^{4}He, ^{4}He)^{9}Be reaction. For this reaction, the angular momentum potential barrier is shown as a dashed line for $l = 6$. r_c and r_s are the corresponding core and shell radii.

A. Formulation of the TRM

To formulate the TRM, the nuclear interaction potentials between the α particle and the core and shell regions of the colliding nucleus, are taken as constant negative radial potentials**,** as shown in Fig. 2. The stationary scattering wave function, $\Psi(r, \theta, \phi)$, for the radial potential can be determined from the usual Schrödinger's equation:

$$-\frac{\hbar^2}{2\mu}\nabla^2\Psi(r,\theta,\phi) + V(r)\Psi(r,\theta,\phi) = E\Psi(r,\theta,\phi), \quad (1)$$

where r is the radial separation between the centers of the target nucleus and the α particle; θ, ϕ are the angular components of the separation vector; μ is the reduced mass between the two nuclei; E is the center-of-mass channel energy. Since it is assumed that $V(r)$ only has radial dependence, the wave function can be expanded in a sum of components of angular momentum quantum numbers, l, each weighted with a radial wave function $R(l, r)$.

$$\left[-\frac{\hbar^2}{2\mu}\left(\frac{\partial}{\partial r^2} + \frac{2}{r}\frac{\partial}{\partial r} - \frac{l(l+1)}{r^2}\right) + V(r)\right]R(l,r) = ER(l,r). \quad (2)$$

The advantage of using constant nuclear potentials is that the $R(l, r)$ functions can be expressed using the well-known spherical Hankel functions. The spherical Hankel functions, $h_1(l, kr), h_2(l, kr)$ are the outgoing and incoming components of the wave functions in the nuclear core and shell regions, and k_0 and k_1 are the wave numbers within the core and shell. The functions $hc_1(l, k_i r), hc_2(l, k_i r)$ are the components of the Coulomb wave function beyond the nuclear potentials, where k_i is the wave number at $r \to \infty$. For the scattering situation shown in Fig. 2, the wave function in the three radial regions have different characteristics, but the amplitudes and slopes must match at the two boundaries. These boundary conditions define a set of equations that can be used to determine the amplitude of the outgoing Coulomb wave relative to the input Coulomb wave. From this outgoing amplitude, the elastic scattering matrix element can be determined in analytical form, and so the differential elastic cross section. By varying these geometrical parameters of the potentials, and comparing the calculated cross sections to experimental values, the optimum parameters of the potentials can be obtained for a particular reaction. From this parameter set, it is then possible to calculate the probability amplitude in the shell region to investigate the occurrence of possible resonances within the shell, i.e., the analog of the whispering gallery phenomena. The mathematical form of the elastic S matrix element, in terms of the physical parameters of the nuclear core and shell, is quite complicated. So, to emphasise the physics in the main text, the mathematical details have been assigned to the Appendix.

III. TRM INTERPRETATION OF ELASTIC DATA FOR ^{4}He SCATTERING FROM ^{9}Li

Using the analytical approach mentioned above (see the Appendix for a detailed description), three sets of published experimental cross section data of α (^{4}He) scattering from weakly bound ^{9}Be, unstable ^{9}Li, and halo ^{6}He nuclei have been used to investigate the applicability of the TRM. In particular, to determine if evidence can be established that suggests shell resonances can occur that can be related to the whispering gallery phenomenon in nuclear scattering.

The first reaction considered is: ^{4}He(^{9}Li, ^{9}Li)^{4}He. Structure calculations of the neutron rich ^{13}B nucleus by Kanada-En'yo *et al.* [31], indicate that at medium excitation energies, states could be identified that resemble a two-cluster configuration, for example, ^{9}Li plus ^{4}He. Since these states are well above the energy threshold for α decay, they will have large energy widths. This strongly suggests that inversely, if an α particle is incident on a ^{9}Li nucleus, at excitation energy near the cluster states in ^{13}B, transient molecular orbiting may occur. The excitation functions for the reaction ^{4}He(^{9}Li, ^{9}Li)^{4}He have been measured at TRIUMF [32] for three angular regions and are shown in Fig. 3. There are two broad resonance structures between center of mass, c.m., energies, $E_{\text{c.m.}}$, 4.7–6.7 MeV and 7–9.5 MeV.

Efforts to interpret this data set, within the compound nucleus (CN) picture, using conventional R-matrix analysis [33], or a single nuclear optical model scattering potential, proved unsuccessful. Since Kanada-En'yo *et al.* [31] structure calculations for ^{13}B indicated that molecular orbiting could be occurring, was the reason why the TRM was introduced that specifically allowed the possibility for orbiting in the extended two-neutron skin of ^{9}Li.

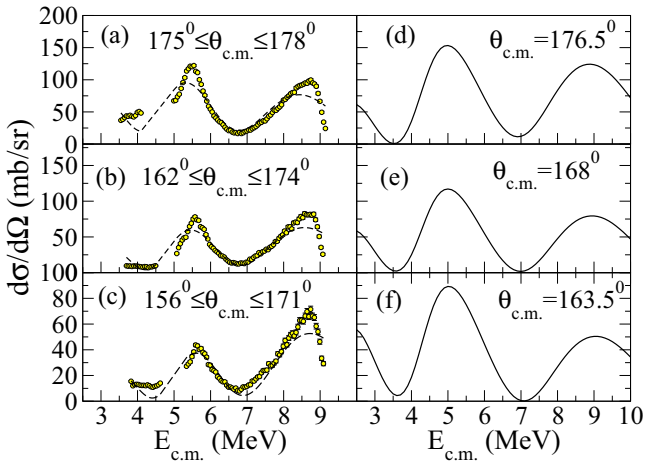

FIG. 3. Left: Differential cross-section data for the reaction ^{4}He(^{9}Li, ^{9}Li)^{4}He [32], expressed as a function of reaction $E_{\text{c.m.}}$. (a) Corresponds to data collected between c.m. angles, $\theta_{\text{c.m}}$: 175°–178°, (b) 162°–174°, (c) 156°–171°. The dashed curve is an optical model fit as explained in the text. Right: TRM calculations at the corresponding mean c.m. angles of (d) 176.5°, (e) 168°, and (f) 163.5°.

The corresponding excitation functions calculated by the TRM, also indicate that there should be two broad resonances near the energy regions where the resonances appear. For this TRM calculation, the radial size of both the core and shell potentials were taken from Kanada-En'yo *et al.* [31]; the strength of the core and shell potentials were varied to reproduce, as near as possible, the magnitude of the experimental cross sections. This optimization resulted in a reasonable agreement between the magnitude of the calculated and experimental cross section as can be seen in Fig. 3, thus confirming that the observed resonances are not core resonances, i.e., coming from the CN. Guided by the TRM philosophy of using two distinct potential regions for the core and shell, a nuclear optical model calculation, using the code FRESCO [34], with two distinct W-S potentials, produced a reasonable fit to the data shown as dashed line in Figs. 3(a)–3(c). The parameters of this nuclear optical model fit are similar to the TRM parameters, except the radius of the shell potential for the nuclear optical model fit is somewhat larger than that needed by the TRM. An important point to note here is that using a single potential with a diffused surface did not produce a satisfactory fit to the data using the code FRESCO [34]. This therefore seems to support the posit that two distinct potential regions are needed for the nuclear core and outer shell nucleons.

A. Probability density and flux

Since the TRM specifically highlights the importance of the outer shell in trapping and transient orbiting, the question then arises: do resonances occur in the outer shell, similar to the whispering gallery phenomena in acoustic and optical systems? The TRM formalism provides a complete description of the wave nature of the scattering process. Therefore, it is possible to calculate the probability intensity of the scattered wave within the core and shell, i.e., $|\Psi(r,\theta,\phi)|^2$. In addition, using this wave function, the flux of probability can also be calculated, which can give additional insight into the reaction mechanism, and in particular, to investigate if whispering gallery resonances are occurring. Since the TRM gives a reasonable representation of the experimental cross section data, the model can be used to investigate the possibility of outer shell resonances leading to partial orbiting, since the experimental data at backward angles show rapid changes in cross sections with incident kinetic energy, Fig. 3. These rapid changes could be associated with such resonances in the shell. The TRM that best fits the data can be used to derive analytical functions for the probability intensity, $P(r,\theta,\phi)$ [Eq. (3)], and probability flux, $F(r,\theta,\phi)$ [Eq. (4)]. These two physical quantities are related to the TRM wave function $\Psi(r,\theta,\phi)$ by the relationships:

$$\mathrm{P}(r,\theta,\phi) = |\Psi(r,\theta,\phi)|^2 \tag{3}$$

$$\mathrm{F}(r,\theta,\phi) = \frac{i\hbar}{2\mu}(\Psi\nabla\Psi^* - \Psi^*\nabla\Psi). \tag{4}$$

For a situation where all scattering potentials are zero, $\Psi(r,\theta,\phi) = e^{i(\bar{r}\cdot\bar{k})}$, so $\mathrm{P}(r,\theta,\phi) = 1.0$ and $F(r,\theta,\phi) = 1 \times \frac{k\hbar}{\mu}$ = probability × velocity, i.e., the probability intensity and flux have constant values over spatial dimensions. This is an important check for any scattering theory.

B. TRM probability density and flux results for ^{4}He(^{9}Li, ^{9}Li)^{4}He

As discussed above, the experimental measurement of the ^{4}He(^{9}Li, ^{9}Li)^{4}He excitation function at backward angles shows a resonancelike structure corresponding to $E_{\text{c.m.}} = 8.7$ MeV (see Fig. 3). The TRM parameters for this reaction have been determined in a previous work [32] and are listed in Table I. The Appendix provides also formalism as to how to calculate values of the wave function from these parameters. From this, the probability amplitude $P(r,\theta,\phi)$, and probability flux $F(r,\theta,\phi)$ have been calculated for this reaction at the resonance energy corresponding to $E_{\text{c.m.}} = 8.7$ MeV [32].

Figure 4 shows the TRM results for $P(r,\theta,\phi)$ and $F(r,\theta,\phi)$ using these potential parameters. Figures 4(a) and 4(b) are the TRM results when the calculation includes Coulomb and nuclear core potentials, but the shell potential is set to zero; Figs. 4(c) and 4(d) are the TRM results when the calculation includes all Coulomb, nuclear shell, and core potentials.

Figure 4 shows various interesting phenomena. Focusing on the top two diagrams, where there is no shell potential, it shows the incoming α wave interacting with the deep potential of the core, located inside the inner red circle. The probability intensity $P(r,\theta,\phi)$ rises to over 1.6 units for the strong upstream reflected wave. As noted above for a null scattering situation, the probability intensity, $P(r,\theta,\phi)$, will be unity at all positions. The dashed lines show the location of the crests for these reflected waves. The separation of these crests is equal to $\lambda/2$, where λ is the incoming wavelength just outside the core. This demonstrates that these are standing waves produced by the reflected wave interfering with the incoming wave. This reflection, in addition, creates a shadow

TABLE I. The TRM potential parameters for the reactions considered in this paper. The parameters a and b are discussed below.

Reaction	Elab (MeV)	r_c (fm)	r_s (fm)	V_c (MeV)	V_i (MeV)	V_s (MeV)	a	b (rad)
$\alpha(^9\mathrm{Li}, ^9\mathrm{Li})\alpha$	32	3.40	5.1	−148.0	−33.0	−13.16	0.0	0.0
$\alpha(^6\mathrm{He}, ^6\mathrm{He})\alpha$	29	3.54	4.51	−174.20	−15.59	−20.55	0.4420	2.2262
$^9\mathrm{Be}(\alpha,\alpha)^9\mathrm{Be}$	10	3.79	5.26	−103.56	−44.33	−14.17	0.1433	3.3920
$^9\mathrm{Be}(\alpha,\alpha)^9\mathrm{Be}$	11	3.58	4.96	−145.66	−15.18	−17.73	0.1588	3.5402
$^9\mathrm{Be}(\alpha,\alpha)^9\mathrm{Be}$	12	4.02	5.27	−152.25	−18.84	−20.61	0.0291	1.9162
$^9\mathrm{Be}(\alpha,\alpha)^9\mathrm{Be}$	14	3.80	5.41	−168.32	−25.19	−8.27	0.0486	6.0517
$^9\mathrm{Be}(\alpha,\alpha)^9\mathrm{Be}$	17.5	4.23	5.34	−112.03	−12.85	−20.23	0.0783	5.5516
$^9\mathrm{Be}(\alpha,\alpha)^9\mathrm{Be}$	20	3.91	5.32	−129.64	−10.06	−12.83	0.0989	1.0241

downstream of the core (it is interesting to note that similar upstream standing waves can often be seen from small objects that interrupt the flow of a slow smooth shallow river). The corresponding flux diagram for this scattering situation shows that, as the flux penetrates into the core, it diminishes. This is expected since the core potential has an imaginary component (see Table I), the value of which will decrease the flux by over 95% by the time it reaches the core center. It is important to emphasize that the TRM does not account for resonances that can originate from core absorption, i.e., compound nucleus resonances.

The bottom two diagrams show that the scattering pattern dramatically changes when a shell potential is present. The location of the shell is between the two red circles. There are still upstream standing waves caused by reflection of the incoming wave, but now a component of the incoming wave becomes trapped in the shell and rotates around it. Further, there appears to be a standing wave within the

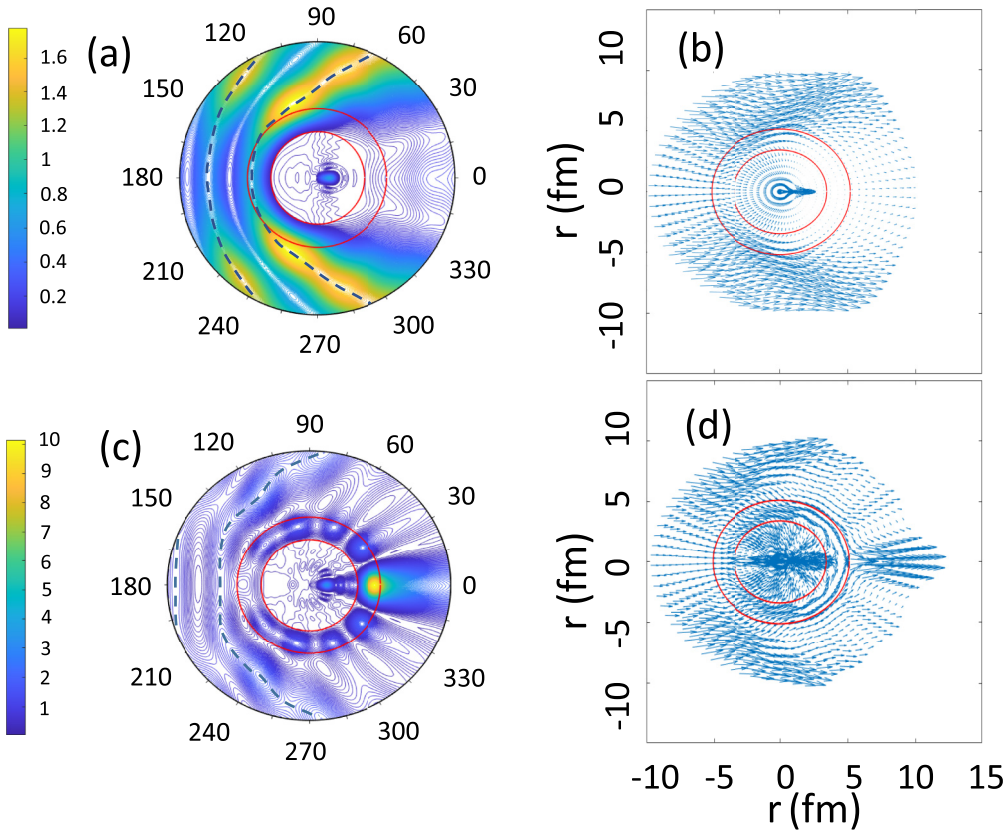

FIG. 4. TRM probability intensity, $P(r,\theta,\phi)$, and probability flux, $F(r,\theta,\phi)$, calculated for the $^9\mathrm{Li}(^4\mathrm{He}, ^4\mathrm{He})^9\mathrm{Li}$, corresponding to $E_{\mathrm{c.m.}} = 8.7$ MeV. (a) $P(r,\theta,\phi)$ and (b) $F(r,\theta,\phi)$ when the TRM includes the Coulomb and only the nuclear core potential. (c) $P(r,\theta,\phi)$ and (d) $F(r,\theta,\phi)$ when the TRM includes all potentials (see text for details). The inner red circle radius ($r_c = 3.4$ fm) corresponds to the core potential radius, and outer circle radius ($r_s = 5.1$ fm) corresponds to the shell radius; the outer circle has no relevance when the shell potential is zero. $P(r,\theta,\phi)$ is plotted as contours of equal intensity at (r,θ) points. The beam is going from left to right. $F(r,\theta,\phi)$ is represented by vectors at (r,θ) points, the vector length corresponding to the flux magnitude along the vector direction.

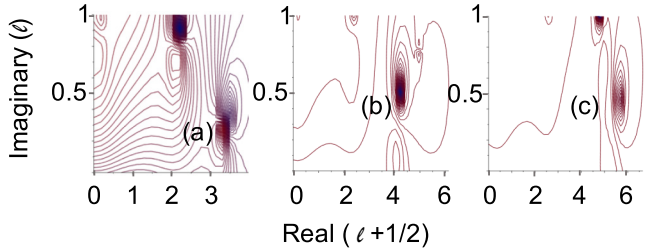

FIG. 5. Angular momentum plane intensity profiles of the modulus of the elastic scattering matrix element at the resonant energies shown in Figs. 3(d)–3(f). (a) Corresponds to a pole at $E_{\text{c.m.}} = 2.4$ MeV, $l = 3$; (b) Corresponds to a pole at $E_{\text{c.m.}} = 5$ MeV, $l = 4$; (c) corresponds to a pole at $E_{\text{c.m.}} = 8.7$ MeV, $l = 5$ [32].

shell, likely caused by the fluxes on opposite shell sides constructively interfering. Previous work [32], indicated that the resonance at $E_{\text{c.m.}} = 8.7$ MeV has a most likely angular momentum quantum number $l = 5$ (see Fig. 5). This would seem to be consistent with the pattern of $P(r, \theta, \phi)$ shown in the diagram, since the number of peaks or nodes around the shell is 2×5; this indicates a coherent linkage between Fig. 4 and Fig. 3. There are components of flux being drawn into the core from the shell, but equally that there is flux being drawn back from the core, and ejected into the forward mode where $P(r, \theta = 0, \phi)$ gains a large value of 10 units. This is an interesting observation since similar focusing at the shell exit region has been observed in similar geometrical configurations for optical (so-called nanojets, [4]), and acoustic systems [2,3]. Hence, such a concentration of wave intensity created by spherical objects seems to be a generic wave phenomenon. Interestingly, this concentration of probability intensity within the shell region, with a modal-like resonance structure, is similar but not identical to Fig. 1, corresponding to the optical case, where the electric field strength at a point is expressed as a ratio to the mean electric field strength. To draw the similarity as close as possible, the Mie calculation for Fig. 1, used the same relative ratio between radii and wavelength as for the nuclear case in Fig. 4. Further, for Fig. 1, the refractive indices used for the core and shell regions, produced the same relative reduction in wavelength within the core and shell, as for the nuclear case in Fig. 4. The electric field intensity pattern shown in Fig. 1, is sensitive to the refractive indexes used, so that there is not an exact match is not too surprising, nevertheless, the similarity is striking.

Given that the TRM provides some guidance to the reaction mechanism, it is possible to inspect the analytical structure of the elastic S-matrix element in the complex angular momentum plane. Resonances will appear as distinct singularity poles in this complex plane, where the value of the imaginary component of a pole is related to the lifetime of the resonance. Inspection of the TRM elastic S-matrix element that best represents the data (Fig. 5), shows two distinct singularity poles whose properties are $l = 5$, lifetime 1.68×10^{-22} s for the upper 8.7 MeV resonance, and $l = 4$, 1.94×10^{-22} s for the 5 MeV lower resonance. For these lifetimes, and using a semiclassical treatment of the rotating flux within the outer shell, the rotating $^9\text{Li} + ^4\text{He}$ system breaks apart before half a

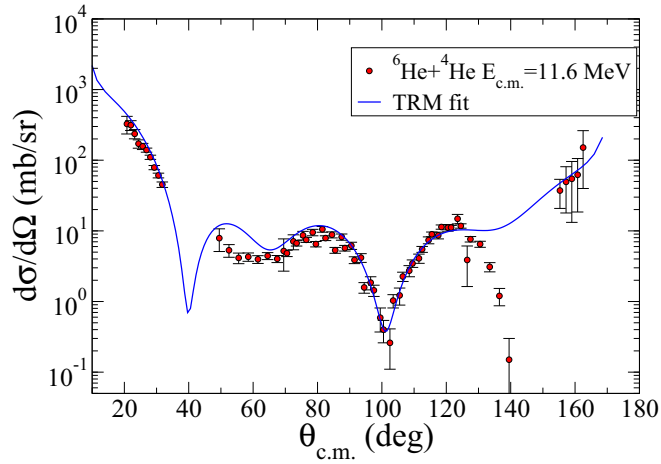

FIG. 6. The $^4\text{He}(^6\text{He}, ^6\text{He})^4\text{He}$ reaction at center of mass energy, $E_{\text{c.m.}} = 11.6$ MeV. Circles are data points from two separate experiments, the first using a ^{4}He gas cell target and the second an implanted ^{4}He solid target, Raabe *et al.* [35,36]. In general, there is consistency between the two data sets, except in the angular range 130–150 degrees, where data from only the gas target could be collected, but with a greater uncertainty. The line is the best TRM fit to the data.

rotation is completed. This is consistent with the information that can be deduced from Fig. 4.

IV. TRM INTERPRETATION OF DATA FOR α SCATTERING FROM ^{6}He AND ^{9}Be

As a further test for the model, two other reactions have been considered involving ^{9}Be and ^{6}He targets, since both ^{6}He and ^{9}Be nuclei have extended neutron shells outside ^{4}He structured cores. Therefore, the TRM has been used to interpret experimental data for ^{4}He scattering from these nuclei.

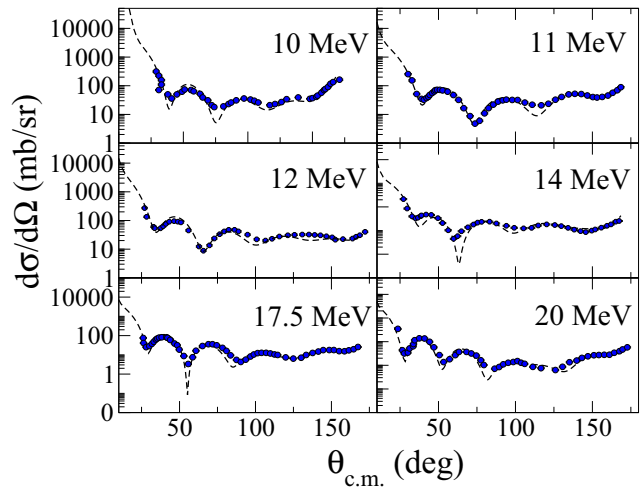

FIG. 7. $^9\text{Be}(^4\text{He}, ^4\text{He})^9\text{Be}$ reaction at six laboratory energies from 10–20 MeV. Circles are data points from Ref. [37]. Dashed lines are best TRM fits to the data.

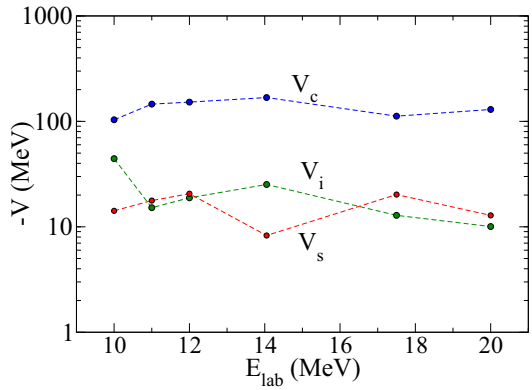

FIG. 8. The strength of the nuclear potentials for the best fits of the TRM to the angular distribution data shown in Fig. 7.

The results are shown in Figs 6 and 7. It can be seen that the TRM, with reasonable potential parameters, discussed in the next paragraph, provides a good representation of the cross sections at the majority of data points for these two reactions. This gives some confidence concerning the value of the TRM approach to interpret reactions of this type.

The TRM potential parameters that have been derived to best match the data for the three reactions considered in this paper are given in Table I. For ^{9}Be(^{4}He, ^{4}He)^{9}Be and for ^{9}Li(^{4}He, ^{4}He)^{9}Li reactions, the spin-orbit interaction was not considered. This, as discussed in Refs. [32,37], could play a role, adding an additional shell potential, which is angular momentum dependent.

V. TRM POTENTIAL PARAMETERS

The potential parameters for the three reactions discussed in this paper are given in Table I, and in Fig. 8 and Fig. 9.

In the case of the ^{4}He(^{6}He, ^{6}He)^{4}He reaction, testing if the simple TRM model can provide some description of the dynamics, it is important to consider the two-neutron exchange which, if direct, is equivalent to the incoming α particle (in the center of mass), exchanging with the α within the ^{6}He target. Some account of this exchange can be implemented by coherently adding the scattering amplitudes, $f(\theta)$, of these

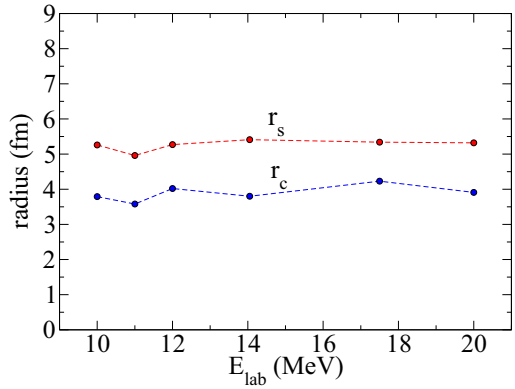

FIG. 9. Potential core and shell radii for the best fits of the TRM to the angular distribution data shown in Fig. 7.

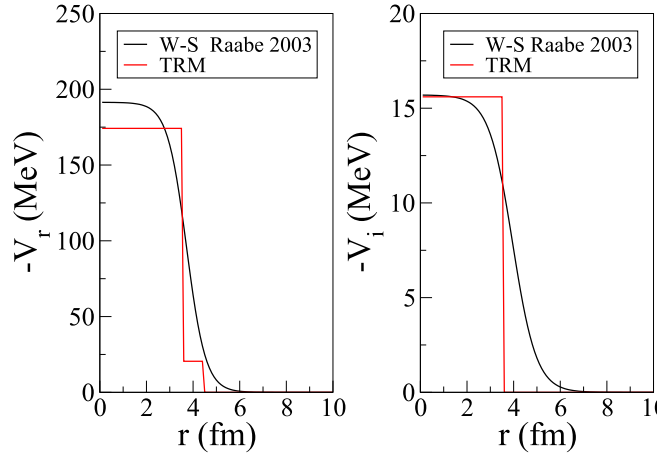

FIG. 10. Comparison of the real and imaginary W-S potential (black line) from Ref. [36], to the TRM potential (red line) for the reaction ^{4}He(^{6}He, ^{6}He)^{4}He. Laboratory ^{6}He beam energy equals 29 MeV.

two components:

$$f(\theta) = f_{\rm el}(\theta) + ae^{ib} f_{\rm el}(\pi - \theta), \tag{5}$$

where a, b are determined by the probability of exchange [38]. For ^{4}He + ^{4}He scattering $a = 1, b = 0$. For the ^{6}He + ^{4}He case, a and b could be angle and channel energy dependent, but for this initial study only the channel energy dependence was considered. The values of a and b for each energy were determined by the best fit to the data for the ^{6}He and ^{9}Be reactions.

For the ^{9}Li reaction, the TRM values for the radii of the core and shell potentials are taken from Ref. [31]. The magnitude of the potentials shown in Table I, corresponds to the best TRM fit to the data shown in Fig. 3. For this analysis no exchange component of the scattering amplitude was needed. Further discussions of this reaction can be found in Ref. [32].

For the ^{6}He reaction, it is interesting to contrast the TRM parameter results with the ones from the analysis of Raabe *et al.* [36]. These authors used the distorted wave Born approximation (DWBA) formalism with W-S potentials to calculate the differential cross section; the parameters of the potential were varied until the calculated values best matched the experimental measurements. Figure 10 shows a comparison of this W-S potential, real and imaginary components, with the TRM potential shown in Table I. The TRM square potentials seem to follow the general trend of the W-S potential, although there are obvious differences especially in the surface region. The value of the complex W-S potential for radii >3.5 fm is significantly above that which is required by the TRM. For the TRM if a complex potential greater than |0.04| MeV is introduced to the shell potential then the shell potential resonance structure rapidly disappears. From a TRM perspective, this means that the wave component that mostly is confined to the shell region, is reemitted outside the shell before it inelastically scatters to other channels.

The TRM potential parameters for the ^{9}Be reaction, are shown in Figs. 8 and 9. There is obviously a variation of the parameter values with beam energy. There is a small

indication that the complex potential is slowly decreasing with energy, while the shell potential does not. Interestingly, the size of the outer shell, $(r_s - r_c)$, remains approximately constant with beam energy. Another interesting point from Table I is the magnitude of the exchange component of the scattering amplitude. The highest magnitude at $a = 0.44$ is found for the ^{6}He reaction. It is smaller for the ^{9}Be reaction, and tends to decrease with beam energy. Since the configuration of ^{6}He is close to ^{4}He, then the exchange component for the ^{6}He would be expected to be close to the reaction $^4\text{He} + ^4\text{He}$, where $a = 1.0$. For the reaction involving ^{9}Be, this nucleus is obviously more complex than ^{4}He, so the exchange potential is expected to be less, as seems to be the case. In summary, the analysis reported here exhibits evidence that, indeed, the TRM provides a reasonable representation of scattering of α particles from light nuclei characterized by an outer shell structure, at least for the three reactions considered here.

VI. CONCLUSIONS

The main theme of this paper is to report on an investigation to understand if resonant surface phenomena like those seen in optical and acoustic systems, can occur for nuclear systems especially if they have extended diffuse surfaces, i.e., a shell outside the core. The understanding of these dynamic effects can be important in the analysis of scattering data with the aim of extracting nuclear structure information.

We know stable nuclei are either spherical or elliptically shaped, with rapid falloff of nuclear density at the nuclear surface, whereas unstable nuclei can have a similar core shape but valence nucleons may travel beyond the surface of the central core, forming a halo or a skin [10,11]. For the scattering of two particles, the potential is related to the nuclear density; in particular, elastic scattering is a peripheral process, hence, very sensitive to the nuclear density at the surface. Indeed, important effects, related to the diffuse nuclear shell of halo nuclei have been observed in elastic scattering of such nuclei [30]. Consequently, quasimolecular resonances could occur in peripheral partial waves and the resonance could be considered as a decaying shell wave propagating around the region of strong absorption, in such a way that is analogous to light scattering from optical spheres, with shells of different refractive indexes.

Over the years, there has been an impressive development of models to describe nuclear reaction outcomes, ranging from phenomenological models, to models which are based on fundamental multiple nucleon-nucleon interactions between reacting nuclei. Although many of these models are successful in describing reaction data, it is often difficult to acquire a physical picture of the underlining reaction mechanism. The main reason behind the development of the simple TRM model has been to address this problem. The TRM model is simple enough that exact algebraic expressions can be obtained for the reaction scattering amplitude, and the density of the scattering wave function in the various reaction regions. This then can lead to insight into the reaction mechanism.

Although the model is simple in its foundation, it nevertheless can provide a good representation of the differential cross section for the three reactions considered in this paper. Further, by inspection of the wave function for the ^{4}He(^{9}Li, ^{9}Li)^{4}He reaction, using the TRM potential parameters derived from experimental data, for the cross section resonance at reaction energy $E_{\text{c.m.}} = 8.7$ MeV, it has been demonstrated that there is clear evidence of a resonance structure within the shell that is very similar to that seen in optical systems. We would like to emphasize that TRM is used to identify resonances within the shell rather than core resonances. Moreover, these shell resonances can be as large and as relevant in enhancing the cross section as the compound nucleus ones.

During supernova and nova explosions, light elements such as H, He, C, N, O are rapidly transformed to heavier elements, by nuclear reactions, which involve nuclei, which are extremely proton rich or neutron rich [13]. Many of these nuclei have very short lifetimes, and so are expected to have extended low-density nucleon tail beyond a dense nuclear core. Today, one of the reasons for building accelerator facilities to produce short-lived radioactive beams, is to measure in the laboratory some of these nuclear reactions [39,40]. While no doubt it will be possible to measure some of these important reactions, it might not be possible, due to the extreme short lifetimes of the nuclei of interest, to measure others. Therefore, there is an important incentive to understand in general the reaction mechanisms of such nuclei, and in particular, the importance of the extended nuclear surface. This has been the main motivation behind the work reported in this paper.

ACKNOWLEDGMENTS

A.C.S. wishes to thank the Edinburgh Physics and Astronomy school for continued support. A.D.P. wishes to thank INFN for their financial support.

APPENDIX: MATHEMATICAL DETAILS OF THE TRM

The scattering situation relevant to the TRM is illustrated in Fig. 2. The amplitudes of the spherical Hankel components within the nuclear core and shell, and the outgoing Coulomb component, can be related to the amplitude of the incoming Coulomb component by the boundary conditions: (i) the radial wave function must remain finite at $r = 0$; (ii) the value of the amplitude of the wave functions must agree on each side at the boundaries at r_c and r_s; (iii) the derivative of the wave functions on each side of the boundaries must be equal.

These boundary conditions are sufficient to determine the amplitude of the wave function components within the shell, as well as the value of the elastic scattering matrix element, S. To use these conditions, it is necessary to specify the mathematical form of the radial functions.

The spherical Hankel functions are connected to the Hankel functions by the relationships [41]:

$$h_1(l, \rho) = \sqrt{\frac{\pi}{2\rho}}\, H^{\{1\}}\left(l + \frac{1}{2},\ \rho\right), \tag{A1}$$

$$h_2(l, \rho) = \sqrt{\frac{\pi}{2\rho}}\, H^{\{2\}}\left(l + \frac{1}{2},\ \rho\right), \tag{A2}$$

for a specific angular momentum quantum number l, and where $\rho = kr$.

The Coulomb functions [42] are related to the confluent hypergeometric functions of the second kind, $U^+$and U^-:

$$hc_2(l,\rho) = (-2)^{l+1}\rho^l e^{\frac{\pi\eta}{2}-i(\rho+\sigma_l)}U^-\,(l+1-i\eta, 2l+2, -2i\rho), \tag{A3}$$

$$hc_1(l,\rho) = (-2)^{l+1}\rho^l e^{\frac{\pi\eta}{2}+i(\rho+\sigma_l)}U^+\,(l+1+i\eta, 2l+2, -2i\rho), \tag{A4}$$

where σ_l is the Coulomb phase shift, and η the Sommerfeld parameter.

In order to determine the elastic scattering matrix element, the following expressions need to be numerically evaluated at the two potential boundaries. At r_c, these functions are

$$F(l,r_c) = \frac{\left[\frac{d(h_2(l,k_0r))}{\mathrm{dr}}\right]_{r_c} + \left[\frac{d(h_1(l,k_0r))}{\mathrm{dr}}\right]_{r_c}}{[h_2(l,k_0r)]_{r_c} + [h_1(l,k_0r)]_{r_c}}, \tag{A5}$$

$$\beta(l,r_c) = \frac{F(l,r_c)[h_2(l,k_1r)]_{r_c} - \left[\frac{d(h_2(l,k_1r))}{\mathrm{dr}}\right]_{r_c}}{F(l,r_c)[h_1(l,k_1r)]_{r_c} - \left[\frac{d(h_1(l,k_1r))}{\mathrm{dr}}\right]_{r_c}}. \tag{A6}$$

At r_s, the following functions are needed:

$$[Lc_2]_{r_s} = \frac{\left[\frac{d(hc_2(l,k_ir))}{\mathrm{dr}}\right]_{r_s}}{[hc_2(l,k_ir)]_{r_s}}, \tag{A7}$$

$$[Lc_1]_{r_s} = \frac{\left[\frac{d(hc_1(l,k_ir))}{\mathrm{dr}}\right]_{r_s}}{[hc_1(l,k_ir)]_{r_s}}, \tag{A8}$$

$$[Rc_{12}\,(k_ir)]_{r_s} = \frac{[hc_2(l,k_ir)]_{r_s}}{[hc_1(l,k_ir)]_{r_s}}. \tag{A9}$$

Finally, the value of the elastic scattering matrix element can be calculated from these expressions:

$$\mathrm{S_{num}}(l,k_i) = [\mathrm{Rc}_{12}\,(k_ir)]_{r_s}\left(\left[\frac{d(h_2(l,k_1r))}{\mathrm{dr}}\right]_{r_s} - [Lc_2]_{r_s}[h_2(l,k_1r)]_{r_s} - \beta(l,r_c)\left(\left[\frac{d(h_1(l,k_1r))}{\mathrm{dr}}\right]_{r_s} - [Lc_2]_{r_s}[h_1(l,k_1r)]_{r_s}\right)\right), \tag{A10}$$

$$\mathrm{S_{dem}}(l,k_i) = \left(\left[\frac{d(h_2(l,k_1r))}{\mathrm{dr}}\right]_{r_s} - [Lc_1]_{r_s}[h_2(l,k_1r)]_{r_s} - \beta(l,r_c)\left(\left[\frac{d(h_1(l,k_1r))}{\mathrm{dr}}\right]_{r_s} - [Lc_1]_{r_s}[h_1(l,k_1r)]_{r_s}\right)\right), \tag{A11}$$

$$\mathrm{S}(l,k_i) = -\frac{\mathrm{S_{num}}(l,k_i)}{\mathrm{S_{dem}}(l,k_i)}. \tag{A12}$$

The elastic scattering cross section can be immediately calculated using this expression for the scattering matrix element.

The probability intensity and probability flux are calculated from the scattering wave function. To specify the radial component of the wave function in the three potential regions, three constants, $A(l)$, $B(l)$, $C(l)$ are needed. These are

$$\mathrm{A}(l) = \frac{hc_2(l,k_ir_s) + S(l,k_i)hc_1(l,k_ir_s)}{h_2(l,k_1r_s) - \beta(l)h_1(l,k_1r_s)}, \tag{A13}$$

$$B(l) = -A(l)\beta(l), \tag{A14}$$

$$C(l) = A(l)\left(\frac{k_0}{k_1}\right)^{\frac{1}{2}} \times \frac{\left[H^{\{2\}}\left(l+\frac{1}{2},k_1r_c\right) - \beta(l)H^{\{1\}}\left(l+\frac{1}{2},k_1r_c\right)\right]}{\left[H^{\{2\}}\left(l+\frac{1}{2},k_0r_c\right) + H^{\{1\}}\left(l+\frac{1}{2},k_0r_c\right)\right]}. \tag{A15}$$

The l wave component between $0 \leqslant r \leqslant r_c$, $R_0(l,r)$, is given by:

$$R_0(l,r) = C(l)\left(\frac{\pi}{2k_0r}\right)^{\frac{1}{2}}\left[H^{\{2\}}\left(l+\frac{1}{2},k_0r\right) + H^{\{1\}}\left(l+\frac{1}{2},k_0r\right)\right]. \tag{A16}$$

The l wave component between $r_c \leqslant r \leqslant r_s$, $R_1(l,r)$, is given by:

$$R_1(l,r) = A(l)\left(\frac{\pi}{2k_1r}\right)^{\frac{1}{2}}\left[H^{\{2\}}\left(l+\frac{1}{2},k_1r\right) - \beta(l)H^{\{1\}}\left(l+\frac{1}{2},k_1r\right)\right]. \tag{A17}$$

The l wave component between $r_s \leqslant r$, $R_i(l,r)$, is given by:

$$R_i(l,r) = hc_2(l,k_ir) + S(l,k_i)hc_1(l,k_ir). \tag{A18}$$

The total wave function in the three regions may be obtained by summing over all l components, e.g., in the region $0 \leqslant r \leqslant r_c$:

$$\Psi_0(r,\theta) = \frac{1}{2}\sum_{l=0}^{\infty} i^l(2l+1)R_0(l,r)P_l[\cos(\theta)]. \tag{A19}$$

[1] L. Rayleigh, *Theory of Sound*, 1st ed., Vol. II (MacMillan, London, 1878).

[2] E. J. Avital, N. D. Bholah, G. C. Giovanelli, and T. Miloh, Sound scattering by an elastic spherical shell and its can-

cellation using a multi-pole approach, Arch. Acous. **42**, 697 (2017).
[3] J. D. Murphy, J. George, A. Nagl, and H.Uberall, Isolation of the resonant component in acoustic scattering from fluid-loaded elastic spherical shells, J. Acoust. Soc. Am. **65**, 368 (1979).
[4] H. Wang, J. Zhang, X. Wu, and D. Shen, On-resonance photonic nanojets for nanoparticle trapping, Opt. Express **27**, 10472 (2019).
[5] G. Mie, Beitrage zur optik truber medien, speziell kolloidaler metallosungen, Ann. Phys. (N.Y.) **330**, 377 (1908).
[6] Mie calculator, https://physics.itmo.ru/en/mie/nearfield.
[7] K. Ladutenko, U. Pal, A. Rivera, and O. Peña-Rodríguez, Mie calculation of electromagnetic near-field for a multilayered sphere, Comput. Phys. Commun. **214**, 225 (2017).
[8] V. Nesvizhevsky, A. Voronin, R. Cubitt, and K. V. Protasov, Neutron whispering gallery, Nature Phys. **6**, 114 (2010).
[9] G. Alkhazovi, I. Novikov, and Y. Shabelski, Nuclear radii of unstable nuclei, Int. J. Mod. Phys. E **20**, 583 (2011).
[10] I. Tanihata, H. Hamagaki, O. Hashimoto, S. Nagamiya, Y. Shida, N. Yoshikawa, O. Yamakawa, K. Sugimoto, T. Kobayashi, D. E. Greiner, N. Takahashi, and Y. Nojiri, Measurements of interaction cross sections and radii of he isotopes, Phys. Lett. B **160**, 380 (1985).
[11] I. Tanihata, H. Hamagaki, O. Hashimoto, Y. Shida, N. Yoshikawa, K. Sugimoto, O. Yamakawa, T. Kobayashi, and N. Takahashi, Measurements of interaction cross sections and nuclear radii in the light p-shell region, Phys. Rev. Lett. **55**, 2676 (1985).
[12] A. M. Moro, K. Rusek, J. M. Arias, J. Gómez-Camacho, and M. Rodríguez-Gallardo, Improved di-neutron cluster model for ^{6}He scattering, Phys. Rev. C **75**, 064607 (2007).
[13] T. Rauscher, *Essentials for nucleosynthesis and theoretical nuclear astrophysics* (Institute of Physics Publishing, London, 2020).
[14] P. Braun-Munzinger and J. Barrette, Dynamical aspects of large angle heavy ion scattering, Phys. Rep. **87**, 209 (1982).
[15] S. Bosanac, Contribution of orbiting to differential cross sections, Phys. Rev. A **19**, 125 (1979).
[16] S. Landowne, Structure in backward-angle excitation functions for strongly absorbed particles, Phys. Rev. Lett. **42**, 633 (1979).
[17] R. Fuller, Quasimolecular state and regge poles, Nucl. Phys. A **216**, 199 (1973).
[18] T. Tamura and H. Wolter, Regge description of optical-model scattering, Phys. Rev. C **6**, 1976 (1972).
[19] A. Arima, G. Scharff-Goldhaber, and K. McVoy, Possible quasi-molecular rotational bands in sd-shell nuclei, Phys. Lett. B **40**, 7 (1972).
[20] K. McVoy, Regge poles and strong absorption in heavy-ion and α-nucleus scattering, Phys. Rev. C **3**, 1104 (1971).
[21] D. Sokolovski, A. Msezane, Z. Felfli, S. Ovchinnikov, and J. H. Macek, What can one do with regge poles? Nucl. Instrum. Meth. B **261**, 133 (2007).
[22] W. Friedman and K. McVoy, A resonant interpretation of gross structure in ^{12}C + ^{12}C and ^{16}O + ^{16}O inelastic scattering, Phys. Lett. B **87**, 179 (1979).
[23] A. Cowley and G. Heymann, Regge pole analysis of the elastic scattering of α-particles from ^{16}O, Nucl. Phys. A **146**, 465 (1970).
[24] L. Satpathy, Nuclear molecular resonances, Prog. Part. Nucl. Phys. **29**, 327 (1992).
[25] O. Dragun and H. Uberall, Nuclear rayleigh and whispering gallery waves excited in heavy ion collisions, Phys. Lett. B **94**, 24 (1980).
[26] D. Saxon and R. D. Woods, Diffuse surface optical model for nucleon-nuclei scattering, Phys. Rev. **95**, 577 (1954).
[27] W. Dickhoff and R. J. Charity, Recent developments for the optical model of nuclei, Prog. Part. Nucl. Phys. **105**, 252 (2019).
[28] N. V. Antonenko, G. Adamian, and V. Sargsyan, Double-folding nucleus-nucleus interaction potential based on self-consistent calculations, Eur. Phys. J. A **58**, 211 (2022).
[29] V. S. Vasilevsky, F. Arickx, J. Broeckhove, and T. Kovalenko, A microscopic three-cluster model with nuclear polarisation applied to resonances of ^{7}Be and the reaction ^{6}Li(p, ^{3}He)^{4}He, Nucl. Phys. A **824**, 37 (2009).
[30] A. Di Pietro, G. Randisi, V. Scuderi, L. Acosta, F. Amorini, M. J. G. Borge, P. Figuera, M. Fisichella, L. M. Fraile, J. Gomez-Camach, H. Jeppesen, M. Lattuada, I. Martel, M. Milin, A. Musumarra, M. Papa, M. G. Pellegriti, F. Perez-Bernal, R. Raabe, F. Rizzo *et al.*, Elastic scattering and reaction mechanisms of the halo nucleus ^{11}Be around the coulomb barrier, Phys. Rev. Lett. **105**, 022701 (2010).
[31] Y. Kanada-Enýo, Y. Kawanami, Y. Taniguchi, and M. Kimura, Cluster states in ^{13}B, Prog. Theor. Phys. **120**, 917 (2008).
[32] A. Di Pietro, A. C. Shotter, J. P. Fernández-García, P. Figuera, M. Fisichella, A. M. Moro, M. Alcorta, M. J. G. Borge, T. Davinson, F. Ferrera, A. M. Laird, M. Lattuada, N. Soić, O. Tengblad, D. Torresi, and M. Zadro, Hints of quasi-molecular states in ^{13}B via the study of ^{9}Li - ^{4}He elastic scattering, Phys. Lett. B **832**, 137256 (2022).
[33] A. M. Lane and R. G. Thomas, R-matrix theory of nuclear reactions, Rev. Mod. Phys. **30**, 257 (1958).
[34] I. Thompson, Fresco code, http://www.fresco.org.uk/.
[35] R. Raabe, A. Piechaczek, A. Andreyev, D. Baye, W. Bradfield-Smith, S. Cherubini, T. Davinson, P. Descouvemont, A. Di Pietro, W. Galster, M. Huyse, A. M. Laird, J. McKenzie, W. F. Mueller, A. Ostrowski, A. Shotter, P. Van Duppen, and A. Wöhr, Elastic 2n-transfer in the ^{4}He(^{6}He, ^{6}He)^{4}He scattering, Phys. Lett. B **458**, 1 (1999).
[36] R. Raabe, A. Andreyev, M. Huyse, A. Piechaczek, P. Van Duppen, L. Weissman, A. Wöhr, C. Angulo, S. Cherubini, A. Musumarra, D. Baye, P. Descouvemont, T. Davinson, A. Di Pietro, A. M. Laird, A. Ostrowski, A. Shotter, L. I. Galanina, and N. S. Zelenskaya, 2n-transfer contribution in the ^{4}He(^{6}He, ^{6}He)^{4}He cross section at $E_{\mathrm{c.m.}} = 11.6$ MeV, Phys. Rev. C **67**, 044602 (2003).
[37] R. Taylor, N. Fletcher, and R. Davis, Elastic scattering of 4-20 MeV alpha particles by Be 9, Nucl. Phys. **65**, 318 (1965).
[38] W. von Oertzen and H. Bohlen, Elastic transfer processes in heavy ion scattering, Phys. Rep. **19**, 1 (1975).
[39] NuPECC Long Range Plan 2017 Perspectives in Nuclear Physics, https://www.nupecc.org/lrp2016/Documents/lrp2017.pdf.
[40] A New Era of Discovery: The 2023 Long Range Plan for Nuclear Science, https://nuclearsciencefuture.org/.
[41] M. Abramowitz and I. Stegun, *Handbook of Mathematical Functions* (Dover, Mineola, 1965).
[42] D. Gaspard, Connection formulas between coulomb wave functions, J. Math. Phys. **59**, 112104 (2018).